Annals of Biomedical Engineering, Vol. 7, pp. 203-238, 1979 0191-5649/79/030203-36 $02.00/0

A FOUR PHASE MODEL OF CAPILLARY TRACER EXCHANGE

Robert J. Roselli
and
Thomas R. Harris

Pulmonary Circulation Center
Biomedical Engineering Program
School of Engineering
Vanderbilt University

In previously proposed models of capillary tracer exchange, red cell membranes have usually been assumed to be either infinitely permeable or completely impermeable to tracer molecules. Permeability of the extravascular cellular compartment has been treated previously, but never in conjunction with finite capillary and red cell permeability effects. Our objective was to examine the situation encountered with multiple indicator experiments in which tracer exchange may be limited by red cell, tissue and capillary membranes. A four phase model is presented which accounts for plasma, red cell, interstitial, and extravascular cellular regions. Results from this model indicate that transcapillary tracer exchange is affected by a minimum of seven dimensionless parameters. The influence of relatively low red cell permeability is most pronounced when the dimensionless capillary permeability is high (i.e., $\alpha_{cap} \geqslant 1$). Deviations in transcapillary extraction values from those corresponding to infinitely permeable erythrocytes can be kept below 5% when capillary permeability is low (i.e., $\alpha_{cap} \leqslant .15$) by pre-equilibrating the injectate with tracer prior to injection. The additional barrier in the extravascular region necessarily decreases overall transvascular tracer exchange but does not affect extraction values in the vicinity of the appearance time.

INTRODUCTION

A number of mathematical models have been reported in the literature which describe transient exchange of a diffusible tracer between the vascular and extravascular regions of a capillary (10). The two most frequently used models were first presented by Crone (5) and Sangren and Sheppard (13). When used to analyze actual tracer data these models can provide estimates

Supported by NHLBI Grant No. HL 19153 (SCOR in Pulmonary Diseases). This work was done during Dr. Roselli's tenure as an NHLBI Training Grant Fellow (NHLBI Training Grant No. T32-HL 07123).

Requests for reprints may be sent to Robert J. Roselli, Pulmonary Circulation Center, B-3211, Vanderbilt University Medical Center, Nashville, Tennessee 37232.

of important capillary parameters such as flow, vascular volume, extravascular volume and the permeability-surface area product (PS) of the capillary to various tracers. Nearly all of these models are based on the assumption that the capillary vascular region and extravascular region are both homogeneous.

Blood has generally been treated as though its volume were either that of the entire blood volume, when the tracer easily permeates the erythrocytes, or that of the plasma alone, when the red cells are assumed to be impermeable to the exchanging species. The only model presented to date which has included the effects of red cell-plasma tracer exchange on trans-endothelial exchange is that of Goresky et al. (6). Unfortunately their model is based on the assumption that the capillary endothelium is infinitely permeable to the diffusing species and is not useful when an estimate of capillary permeability is desired.

The extravascular tissue region available to the diffusing species has generally been assumed to be either the entire extravascular volume, when the cell membranes do not impede tracer transport, or to be limited to the interstitial space, when the cell membranes are nearly impermeable to the diffusing species. A number of theoretical studies have included separate interstitial and cellular regions within the extravascular space. Rose et al. (11) recently presented a detailed model of capillary, extracellular and intracellular tracer exchange which incorporated the assumptions of plug flow, rapid radial diffusion, negligible red cell exchange and negligible axial diffusion.

Many of the earlier models included simplifications which are generally not applicable to transient multiple indicator studies. For instance, Conn and Robertson (4) and Bellman et al. (2) assumed the capillary extracellular and cellular regions were each well mixed so that tracer concentrations depend on time but not on axial position. Ziegler and Goresky (17) treated the special case when the diffusible tracer is confined to the cellular space after crossing the membrane (potassium and rubidium) while Sheehan and Renkin (14) and Tancredi et al. (15) considered only steady-state transport of these same tracers.

Our primary objective was to develop a mathematical model which describes transient tracer exchange in a capillary where both blood and extravascular volume are heterogeneous and capillary permeability is finite. This model was then used in a subsequent investigation (12) to estimate the effects that finite red cell permeability and finite extravascular cellular permeability have on the standard multiple indicator calculations of extravascular volume and capillary PS.

The Model

In this section we present a heterogeneous model which can be used to predict the concentration-time history of a diffusible indicator as it emerges from a single ideal capillary unit. Each capillary and its surrounding tissue is assumed to be isolated from neighboring capillary units and is not influenced

by tracer transport in adjacent capillaries. This concept was originally proposed by Krogh (9) to describe oxygen transport in tissue and has been adopted by a number of investigators to characterize capillary mass exchange. Use of the Krogh cylinder model simplifies the problem considerably. Instead of treating the entire organ from the onset, we may begin by obtaining the solution for a single capillary unit. The responses of all capillaries can then be combined to obtain the response of the entire organ.

A schematic of our single capillary model is shown in Figure 1. The intravascular region of the capillary unit is divided into two separate components, representing the water volumes occupied by erythrocytes (V_{RC}) and plasma (V_P) respectively. The red cell and plasma phases of the model are separated by an effective diffusion barrier, with surface area S_{RC}, which represents the resistance offered by the erythrocyte membrane to indicator transport. The ease with which tracer molecules can pass through the erythrocyte-plasma diffusion barrier is characterized by the permeability of the barrier, P_{RC}, to the particular tracer selected. The higher the permeability, the less is the resistance offered by the barrier to tracer transport.

The extravascular tissue space of the capillary unit is also divided into two regions, representing the water volumes of the interstitial space (V_I) and cellular space (V_C). These regions are separated by a diffusion barrier of surface area S_C and permeability P_C representing the cellular membranes of the tissue region being used. The plasma and interstitial regions are separated by a third barrier of surface area S_{cap} and permeability P_{cap} which represents the resistance offered by the capillary endothelium.

The following simplifying assumptions are made:

1. The permeabilities of all three barriers (i.e., erythrocyte membrane, capillary endothelium and extravascular cellular membrane) to any particular tracer are allowed to be independent of each other but are assumed to be constant in both time (t) and axial position (x).

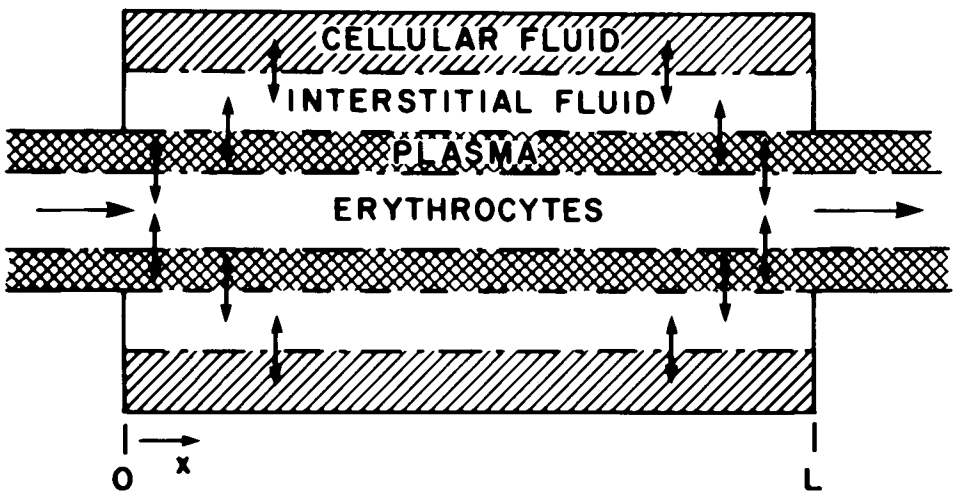

FIGURE 1. Four phase capillary model.

2. The cross-section of the capillary unit can be of arbitrary shape but the volumes per unit length (i.e., the cross-sectional area) of each of the four compartments are assumed not to vary in time or space.
3. Red cell and plasma velocities are assumed to be identical in the model presented here. The effects of allowing these to deviate from each other will be considered in the accompanying article in this issue (12).
4. The convective transport of tracer in the plasma phase is assumed to be much larger than transport by axial diffusion (i.e., $uL/D \gg 1$, where D is the diffusivity of tracer in plasma). The effects of finite axial diffusion and dispersion (i.e., when velocity profiles are not ignored) were examined theoretically by Bassingthwaighte (1) and were generally found to be small. Guller et al. (8) found that their model fit for myocardial sodium tracer data (high diffusivity) was not influenced significantly by large changes in the axial dispersion coefficient.
5. The resistance to diffusion offered by the fluids in each of the four phases is assumed to be negligible in comparison to the resistances offered by the erythrocyte membranes, capillary endothelium or tissue cell membranes. In light of these assumptions, the concentration in any of the four compartments will be independent of radial location and will be a function of time and axial location only. This rapid diffusion is sufficient justification for allowing the cross-section of the capillary unit to have arbitrary shape.
6. The red cell membrane and capillary membrane are assumed to be extremely thin so that no measureable accumulation of indicator occurs within the membranes. Mass transfer across the membrane can then be assumed to be in a quasi-steady state (i.e., the time rate of change of concentration within the membrane is small with respect to the flux through the membrane). Therefore, instantaneous flux through the membrane depends upon the permeability of the membrane to the tracer and the instantaneous concentration difference across the membrane. We will be concerned only with indicators that diffuse passively across the three diffusion barriers so that no carrier systems (concentrating mechanisms) are involved and the rate constants for the influx and efflux for each individual barrier are identical.

In light of the above assumptions, a membrane-limited transport equation can be written for each of the four regions of Figure 1 in terms of the red cell concentration, c_{RC}, plasma concentration, c_P, interstitial concentration, c_I, and extravascular cellular concentrations, c_C:

Red Cell region

$$V_{RC}\left[\frac{\partial c_{RC}}{\partial t} + u\frac{\partial c_{RC}}{\partial x}\right] = P_{RC}\,S_{RC}\,(c_P - c_{RC}) \tag{1}$$

Plasma region

$$V_P\left[\frac{\partial c_P}{\partial t} + u\frac{\partial c_P}{\partial x}\right] = P_{RC}\,S_{RC}\,(c_{RC} - c_P) + P_{cap}\,S_{cap}\,(c_I - c_P) \tag{2}$$

Interstitial region

$$V_I \frac{\partial c_I}{\partial t} = P_{cap} S_{cap} (c_P - c_I) + P_C S_C (c_C - c_I) \tag{3}$$

Extravascular Cellular region

$$V_C \frac{\partial c_C}{\partial t} = P_C S_C (c_I - c_C) \tag{4}$$

The frame of reference is fixed in the stationary capillary endothelium or extravascular volume with x = 0 at the capillary inlet and x = L at the outlet. Equations 1-4 imply that tracer molecules cannot pass between the red cells and the extravascular region unless they first enter the plasma phase. Therefore, the occurrence of red cell-endothelium contact is assumed to be rare or tracer flux is virtually prevented by the combined resistance of the double membrane.

Equations 1-4 are to be solved for the initial conditions:

$$c_p (0,x) = c_{RC} (0,x) = c_I (0,x) = c_C (0,x) = 0 \tag{5}$$

and boundary conditions:

$$\begin{aligned} c_p (t,0) &= c_{po} (t) \\ c_{RC} (t,0) &= c_{RCo} (t) \end{aligned} \tag{6}$$

where c_{po} (t) and c_{RCo} (t) are known input concentrations in the plasma and red cell phases respectively, at x = 0.

We were interested in two particular forms of the boundary condition, Eq. 6. The first was an ideal Dirac impulse in each of the plasma and red cell phases at x = 0:

$$\begin{aligned} c_p (t,0) &= \frac{m_{i,p}}{F_p} \delta (t) \\ c_{RC} (T,0) &= \frac{m_{i,RC}}{F_{RC}} \delta (t) = \frac{(m_i - m_{i,p})}{F_{RC}} \delta (t) \end{aligned} \tag{6a}$$

where m_i is the total mass of indicator injected in the pulse, $m_{i,p}$ is the mass injected in the plasma phase alone, $m_{i,RC}$ is the mass injected in the red cell phase alone and F_p and F_{RC} are the plasma and red cell volumetric water flow rates respectively (i.e., $F_p = V_p$ u/L, $F_{RC} = V_{RC}$ u/L). The second set of boundary conditions we employed was chosen to be more representative of the actual shape of indicator curves found at the capillary inlet:

$$\begin{aligned} c_p (t,0) &= c_{p,i} \left(\frac{t}{\bar{t}} \sigma^2 \exp \left(\frac{-\sigma t}{\bar{t}} \right) \right) \\ c_{RC}(t,0) &= c_{RC,i} \left(\frac{t}{\bar{t}} \sigma^2 \exp \left(\frac{-\sigma t}{\bar{t}} \right) \right) \end{aligned} \tag{6b}$$

where $\bar{t}$ is the mean vascular transit time ($\bar{t} = (V_{RC} + V_P)/(F_{RC} + F_P)$), $c_{p,i}$ and $c_{RC,i}$ are constants and σ is a paramter which controls the dispersion of the input function.

Conservation of mass in the plasma and red cell phases at the capillary inlet requires that:

$$m_{i,p} = F_p \int_0^\infty c_{po}(t)\,dt$$

and

$$m_{i,RC} = m_i - m_{i,p} = F_{RC} \int_0^\infty c_{RCo}(t)\,dt$$

substituting Eq. 6b into the above equations we find the constants $c_{p,i}$ and $c_{RC,i}$ are related to the total mass injected and the mass injected in the plasma phase in the following manner:

$$c_{p,i} = \frac{m_{i,p}}{(V_{RC}+V_P)} \quad \frac{F}{F_p}$$

$$c_{RC,i} = \frac{(m_i - m_{i,p})}{(V_{RC}+V_P)} \quad \frac{F}{F_{RC}}$$

It is virtually impossible to measure independently the capillary outlet concentrations c_p (t,L) and c_{RC} (t,L), since the instantaneous separation of red cells and plasma at the capillary exit can not be easily achieved. The quantity measured experimentally at any axial location, x, is the flow-averaged concentration of indicator in the blood, $\bar{c}$ (t,x):

$$\bar{c}(t,x) = \frac{F_p}{F} c_p(t,x) + \frac{F_{RC}}{F} c_{RC}(t,x) \tag{7}$$

At the capillary inlet (x = 0) the flow averaged concentration for the boundary conditions given in Eq. 6a, is:

$$\bar{c}(t,0) = \frac{m_i}{F}\delta(t)$$

and for the boundary conditions of Eq. 6b the flow-averaged concentration is

$$\bar{c}(t,0) = \frac{m_i}{(V_{RC}+V_p)} \left(\sigma^2 \frac{t}{\bar{t}} \exp\left(\frac{-\sigma t}{\bar{t}}\right)\right)$$

If the tracer cannot permeate the capillary endothelium it is said to be a vascular indicator. The concentration-time history at the capillary exit for a vascular indicator is known as the vascular reference curve, c_R (t,L). Since no reference indicator leaves the capillary and no axial diffusion is allowed, the reference curve is simply the flow averaged inlet curve delayed in time by the vascular transit time, $\bar{t}$:

$$c_R(t,L) = 0 \qquad t < \bar{t}$$

$$c_R(t,L) = \bar{c}(t-\bar{t},0),\ t \geqslant \bar{t} \tag{8}$$

Therefore when the red cell and plasma velocities are equal, the reference curve for boundary conditions of Eq. 6a is simply a delayed impulse:

$$c_R(t,0) = \frac{m_i}{F}\delta(t-\bar{t})$$

and for boundary conditions of Eq. 6b the intravascular reference curve is described by:

$$c_R(t,0) = 0,\ t < \bar{t}$$

$$c_R(t,0) = \frac{m_i}{(V_{RC}+V_P)}\,\sigma^2\left(\frac{t}{\bar{t}} - 1\right)\exp\left(-\sigma\left(\frac{t}{\bar{t}} - 1\right)\right),\ t > \bar{t} \tag{8b}$$

Non-Dimensionalization

Introduction of the following quantities

$$X = x/L$$

$$T = t/\bar{t}$$

$$C = \frac{cF\bar{t}}{m_i} = \frac{c(V_{RC}+V_p)}{m_i}$$

into Eqs. 1-4 will produce the dimensionless transport equations:

Red Cells

$$\frac{\partial C_{RC}}{\partial T} + \frac{\partial C_{RC}}{\partial X} = \alpha_{RC}(C_P - C_{RC}) \tag{9}$$

Plasma

$$\frac{\partial C_p}{\partial T} + \frac{\partial C_p}{\partial X} = \beta\alpha_{RC}(C_{RC}-C_p) + (1+\beta)\alpha_{cap}(C_I-C_p) \tag{10}$$

Interstitial Space

$$\gamma\frac{(1-\zeta)}{(1+\beta)}\,\frac{\partial C_I}{\partial T} = \alpha_{cap}(C_P-C_I) + \alpha_C(C_C-C_I) \tag{11}$$

Cellular Space

$$\frac{\gamma\zeta}{(1+\beta)}\,\frac{\partial C_C}{\partial T} = \alpha_C(C_I-C_C) \tag{12}$$

where

$$\alpha_{RC} = \frac{P_{RC}\, S_{RC}}{F_{RC}} = P_{RC}\, \left(\frac{S_{RC}}{V_{RC}}\right) \bar{t}$$

$$\alpha_{cap} = \frac{P_{cap}\, S_{cap}}{F} = P_{cap}\, \left(\frac{S_{cap}}{V_{RC}+V_P}\right) \bar{t}$$

$$\alpha_C = \frac{P_C\, S_C}{F} = P_C\, \left(\frac{S_C}{V_C}\right)\, \left(\frac{V_C}{F}\right)$$

$$\beta = \frac{V_{RC}}{V_P}$$

$$\gamma = \frac{V_I+V_C}{V_P}$$

$$\zeta = \frac{V_C}{V_I+V_C}$$

In the terminology of Rose et al. (11), $\zeta = \theta/(\theta + \gamma)$ where $\gamma = V_I/(V_{RC} + V_P)$ and $\theta = V_C/V_{RC} + V_P)$. The definition of γ used in this article follows the original definition in Goresky et al. (6).

The parameters α_{RC}, α_{cap} and α_C are dimensionless mass transfer coefficients. Each can be multiplied by various combinations of β, γ or ζ to yield different dimensionless parameters but all can be reduced to the product of three separate effects: 1) the permeability, which will depend only on the physical properties of the tracer and the structure of the membrane; 2) a geometric factor, which is the ratio of the surface available for indicator transport to its volume of distribution, and 3) the time required for the indicator to traverse the volume (or membrane contact time). Increasing any of these factors will promote increased tracer exchange.

The dimensionless flow-averaged concentration of indicator in the blood $\bar{C}$ (i.e., the dimensionless form of Eq. 7 is:

$$\bar{C}\,(T,X) = \frac{1}{(1+\beta)}\, (C_p\,(T,X) + \beta\, C_{RC}\,(T,X))$$

The initial conditions in dimensionless form become:

$$C_P\,(0,X) = C_{RC}\,(0,X) = C_I\,(0,X) = C_C\,(0,X) = 0 \qquad (13)$$

while the boundary conditions for the impulse input functions become:

$$C_P\,(T,0) = \mu\,(1+\beta)\,\delta\,(T) \qquad (14a)$$

$$C_{RC}\,(T,0) = \frac{(1-\mu)\,(1+\beta)}{\beta}\,\delta\,(T)$$

or for the more general input conditions of Eq. 6b:

$$C_P(T,0) = \mu(1+\beta)\,\sigma^2\,T\,e^{-\sigma T}$$
$$C_{RC}(T,0) = \frac{(1-\mu)(1+\beta)\,\sigma^2\,T\,e^{-\sigma T}}{\beta} \tag{14b}$$

The parameter μ is the rate at which indicator is deposited in the plasma phase divided by the total rate at which indicator enters the capillary inlet, i.e.,

$$\mu = \frac{C_P(T,0)\,F_P}{\bar{C}(T,0)\,F} = \frac{1}{(1+\beta)}\,\frac{C_P(T,0)}{\bar{C}(T,0)}$$

In general μ can be a function of time. However in our analysis we will assume that the red cells and plasma are injected simultaneously and that their input functions have the same shape. This assumption is implicit in the boundary conditions in Eqs. 14a and 14b. In addition, we assume that the red cells and plasma are separated until they are deposited at the capillary inlet and hence the ratio $C_P(T,0) / \bar{C}(T,0)$ is a constant. Then the above expression for μ after integrating over all time, simplifies to:

$$\mu = \frac{1}{1+\beta}\,\frac{\int_0^\infty C_p(T,0)\,dT}{\int_0^\infty \bar{C}(T,0)\,dT} = \frac{m_{i,p}}{m_i}$$

The dimensionless reference concentration at the capillary exit (X = 1) for an impulse input at X = 0 (i.e., Eq. 8a) is:

$$C_R(T,1) = \delta(T-1) \tag{15a}$$

and for the more general input function (i.e., Eq. 8b) is:

$$C_R(T,1) = \begin{cases} 0, & T<1 \\ \sigma^2(T-1)e \quad (T-1\text{xp}(-\sigma)) & T \geqslant 1 \end{cases} \tag{15b}$$

Finding general analytic solutions to Eqs. 9-13 and either 14a or 14b would be a formidable task. Each of the four dependent variables C_P, C_{RC}, C_I and C_C are functions of two independent variables, X and T, and seven dimensionless parameters α_{RC}, α_{cap}, α_C, β, γ, μ and ζ. If the more general boundary conditions of Eq. 14b are used, then an eighth dimensionless parameter, σ, will also influence the solutions. We did not attempt to obtain analytic solutions. A finite difference technique similar to that employed by

Bassingthwaighte (1) was used to obtain approximate dimensionless concentration-time solutions to Eqs. 9-14 at various axial locations within the plasma, red cell, interstitial and cellular regions. Details are given in the Appendix.

RESULTS

Accuracy of the finite difference method

Generally, for α_{cap} less than 20, the C(T) curves produced with the finite difference techniques were not altered appreciably when the number of axial compartments was increased beyond 20. For higher values of the dimensionless capillary permeability it was necessary to use 40 compartments and occasionally (particularly for impulse responses) we used 80 compartments. The effects of sequentially quadrupling the number of axial compartments per region from 10 to 160 is shown in Table 1. Here, an impulse function at T = 0, X = 0 was approximated by a finite pulse (i.e., all the indicator was initially placed in the first plasma compartment). We chose the dimensionless capillary permeability in this example to be the highest employed in any of our subsequent C(T) presentations (α_{cap} = 10). The other parameters used in constructing Table 1 were $\alpha_{RC} = 3$, $\beta = .5$, $\gamma = 3$ and $\alpha_C \to \infty$ (i.e., a homogeneous extravascular region). We have not included comparision at T = 1 where the dimensionless concentration would theoretically be infinitely large for a Dirac impulse input. The maximum deviation of the 10 compartment concentration solutions from the 160 compartment concentrations in Table 1 is less than 10%. In fact, less than 0.7% difference can be found in the solutions tabulated when the number of compartments is greater than or equal to 40.

In Table 2 we compare the finite difference solution when α_{RC} = 10,000 to the Sangren-Sheppard analytic solution given by Goresky et al. (7) for a dimensionless capillary permeability of 10. For this case and for lower values of α_{cap} the finite difference technique is accurate to within one percent.

TABLE 1
Variation in the numerical $\bar{C}$ (T) solution* at the capillary outlet as the number of compartments, IMAX, is increased

T	$\bar{C}$(T)		
	IMAX = 10	IMAX = 40	IMAX = 160
1.2	.1103	.0999	.0993
2.0	.2539	.2400	.2385
3.0	.3171	.3283	.3290
4.0	.2182	.2356	.2370
5.0	.1006	.1023	.1025
6.0	.0350	.0303	.0299

*Impulse response when $\alpha_C \to \infty$, $\alpha_{cap} = 10$, $\alpha_{RC} = 3$, $\beta = .5$, $\gamma = 3$, $\mu = 1$, X = 1.

TABLE 2
Comparison of the exact Sangren-Sheppard solution C* to the finite difference solution* $\bar{C}$ when $\alpha_{RC} = 10^4$

T	C*(T)	$\bar{C}$(T)
1.2	.0219	.0222
2.0	.3095	.3098
3.0	.4375	.4368
4.0	.1955	.1955
5.0	.0471	.0472
6.0	.0076	.0076

*Impulse response when $\alpha_{cap} = 10, \beta = .5, \gamma = 3, \mu = .6667$, IMAX = 80, X = 1, $\alpha_C \to \infty$.

No finite difference technique can truly describe an emerging impulse function at X = 1 and T = 1. The finite element size would have to approach zero for the concentration to become infinitely large. However, we were not interested in calculating the dimensionless concentration at this point (which we knew to be infinitely large), but instead we wanted to calculate the fraction of tracer which could not cross the capillary endothelium and therefore emerged as an impulse at T = 1 (i.e., m/m_i). For a pulse-like input the transmitted mass fraction, can be estimated from the finite difference solution, i.e.,

$$\frac{m}{m_i} \approx \bar{C}(1,1)\,\Delta T$$

The mass fraction emerging in the impulse can be determined analytically by solving Eqs. 1-6 when back-diffusion is not allowed. We have compared the emerging mass fraction computed with the finite difference technique (IMAX $\geqslant$ 20) to the analytic solution for various values of α_{cap}, α_{RC} and μ. For all conditions when $\alpha_{cap} = 5.1$ or 1.0 and under most conditions when $\alpha_{cap} = 10$, the two values agree to within 1%. When α_{cap} is 10 and α_{RC} is high the deviation is somewhat greater. This is due to the fact that $\bar{C}(1,1)\,\Delta T$ includes not only the indicator which emerges in the impulse at T = 1 but also any additional mass of indicator which emerges during the interval from T = 1 to T = 1 + ΔT. At high capillary permeabilities, the additional mass emerging during this period may be a significant fraction of $\bar{C}(1,1)\,\Delta T$, since the impulse at T = 1 is very small.

We also compared the finite difference solutions for $\bar{C}$, C_{RC} and C_P when $\alpha_{RC} = 3$, $\gamma = 5$, $\beta = .5$, $\alpha_{cap} = 10^6$ and $\mu = 0$ (Fig. 2) to the analytic solution given by Goresky et al. (6) when $\alpha_{cap} \to \infty$. Although the analytic-finite difference agreement is not as close when $\alpha_{cap} \to \infty$ as it is when $\alpha_{RC} \to \infty$ (i.e., Table 2), the theoretical and finite difference concentrations agree to within 5% for T < 4.6. A more accurate finite difference solution would require more than 80 axial compartments to adequately approximate the delayed step function at T = 6. The largest dimensionless capillary perme-

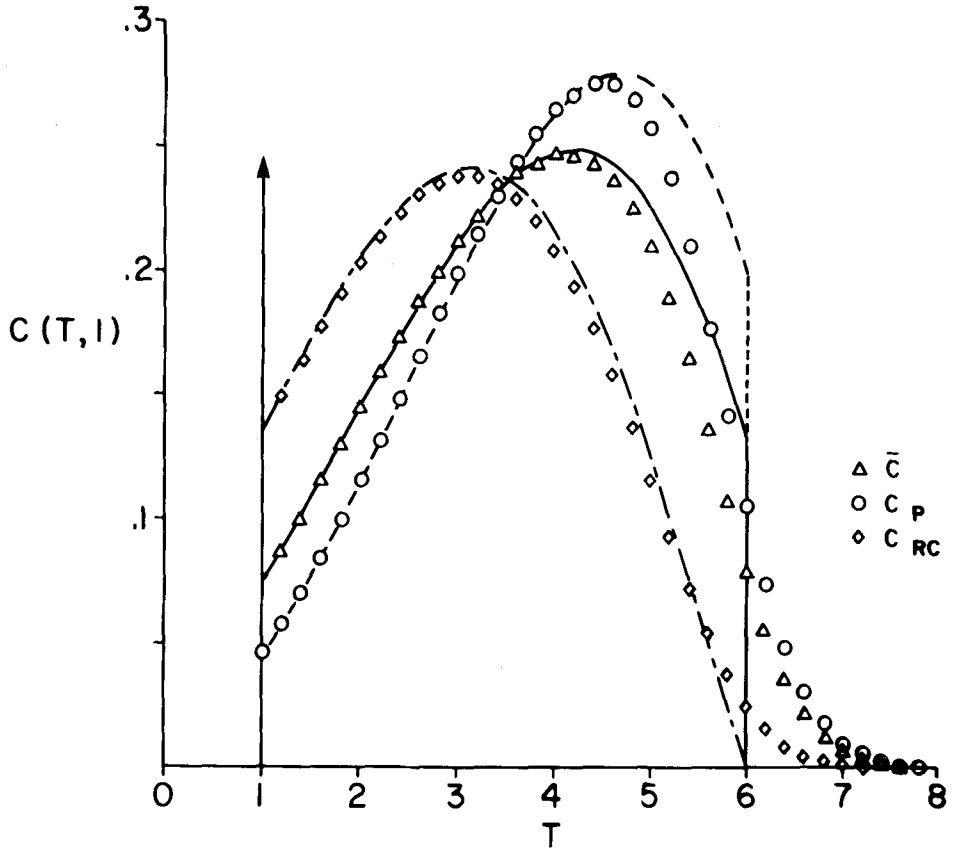

FIGURE 2. Comparison of the finite difference composite ($\bar{C}$), plasma (C_P) and red cell (C_{RC}) concentrations to the corresponding analytic solutions (solid, dashed and hatched lines respectively) of Goresky et al. (6) when $\alpha_{cap} \to \infty$. Finite difference model parameters used were $\alpha_{cap} = 10^6$, $\alpha_{RC} = 3$, $\beta = .5$, $\gamma = 5$, $\mu = 0$, $\alpha_C \to \infty$, IMAX = 80. Impulse area at T = 1 was .0498 for the exact solution and .0505 for the finite difference solution.

ability used in our study was 10 (rather than $\alpha_{cap} \to \infty$) and therefore the finite difference technique was not required to mimic awkward step functions or impulse functions except at T = 1 where it was quite satisfactory.

One final check on the finite difference technique was to compare the first and second moments of several computed curves with the analytic moment solutions given in the appendix of Roselli & Harris (12). In all cases the zeroth, first and second moments computed from the finite difference C(T) curves were within 1% of the value obtained using the analytic solutions.

Model Results

Because there is such a large number of parameters in the model it is not possible to present the effects of varying each here. We will not concern ourselves with variations in extravascular volume, which has been adequately

described by Goresky et al. (7) and Bassingthwaighte (1), or hematocrit value, which has been discussed by Bassingthwaighte (1). Instead we fix the erythrocyte to plasma water volume ratio (β) at 0.5 (i.e., Hct = 40%) and the extravascular to plasma water volume ratio (γ) at 3.0 (which corresponds to an extravascular to vascular water ratio of 2.0), a value characteristic of normal lung tissue.

We believe that it is essential to show impulse responses of the capillary model under various combinations of red cell permeability, microvascular permeability and extravascular cellular permeability. These are presented in the next section. In addition, we shall also present C(T) responses and the corresponding extractions for a more realistic skewed exponential input function.

IMPULSE RESPONSE

Effects of Red Cells

In Figure 3 we present the effects of changing red cell permeability on the impulse response when indicator is injected only in the plasma phase ($\mu = 1$) and the extravascular region is homogeneous ($\alpha_C \to \infty$). In the first set of curves the dimensionless permeability of the capillary endothelium was low (i.e., $\alpha_{cap} = 0.15$) and the dimensionless red cell permeability varied between 10^{-6} and 10^{+6}. The mass of indicator emerging in the impulse at the capillary outlet only changed from 80% of the injected mass (i.e., at X = 0, T = 0) when red cells are impermeabile (i.e., $\alpha_{RC} = 10^{-6}$) to 86% of the initial mass when $\alpha_{RC} = 10^{+6}$. This variation would be even smaller if both erythrocytes and plasma were initially pre-equilibrated with tracer (i.e., $\mu = 1/(1+\beta)$ at X = 0). Note that when red cell permeability lies between these two ex-

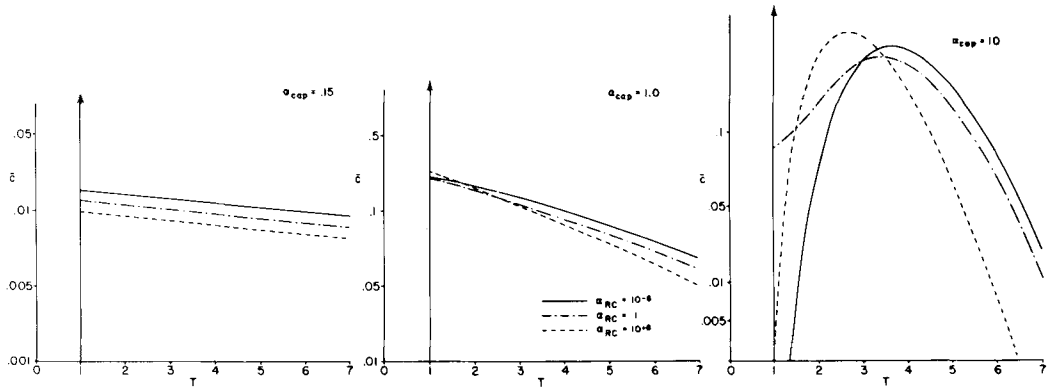

FIGURE 3. $\bar{C}$ vs T for α_{RC} of 10^{-6}, 1 or 10^{+6} and $\beta = .5, \gamma = 3, \alpha_C \to \infty$ and $\mu = 1$. Left: $\alpha_{cap} = .15$. Impulse areas at X = 1, T = 1 are: .7987 ($\alpha_{RC} = 10^{-6}$), .8295 ($\alpha_{RC} = 1$) and .8608 ($\alpha_{RC} = 10^{-6}$), Center: $\alpha_{cap} = 1$. Impulse areas at X = 1, T = 1: .2252 ($\alpha_{RC} = 10^{-6}$), .3142 ($\alpha_{RC} = 1.0$) and .3702 ($\alpha_{RC} = 10$) Right: $\alpha_{cap} = 10$. Impulse areas at X = 1, T = 1: $< 10^{-4}$ ($\alpha_{RC} = 10^{-6}$ and 10^{+6}), .014 ($\alpha_{RC} = 1$).

tremes both the impulse area and the tail (i.e., back-diffusion portion) of the curve lie between the $\alpha_{RC} = 10^{-6}$ and $\alpha_{RC} = 10^{+6}$ impulse responses. The maximum variation in transmitted impulse areas becomes considerably larger when the dimensionless capillary permeability is increased to $\alpha_{cap} = 1$ (i.e., 23% for $\alpha_{RC} = 10^{-6}$ vs. 37% for $\alpha_{RC} = 10^{+6}$). The transmitted impulse area for an intermediate value of α_{RC} still lies between these two extremes but red cell exchange has altered the back-diffusion portion of the curve so that it no longer is bounded at all times by the $\alpha_{RC} = 10^{-6}$ and $\alpha_{RC} = 10^{+6}$ curves.

When the dimensionless capillary permeability is increased to $\alpha_{cap} = 10$ the transmitted impulse areas are negligible (i.e. $<10^{-4}$) at both $\alpha_{RC} = 10^{-6}$ and $\alpha_{RC} = 10^{+6}$. However if $\alpha_{RC} = 1$ then 1.4% of the tracer initially injected at X = 0, T = 0 will emerge in the impulse at X = 1, T = 1. Another interesting phenomenon found at $\alpha_{cap} = 10$ is that although all of the mass was initially injected as an impulse in the plasma phase alone, 94% of the mass emerging in the transmitted impulse is transported in the red cell phase. This is an example of what has been referred to by Chinard et al. (3) as red cell trapping.

A more instructive presentation of the trapping phenomenon may be found in Figure 4 ($\alpha_{RC} = 1$, $\alpha_{cap} = 10$) where a sequence of five axial tracer distributions in the red cell, plasma and extravascular regions are shown. For comparison we also present the same sequence when red cells offer essentially no resistance to diffusion. The tracer is initially deposited as an impulse in the plasma phase at X = 0 and T = 0. Tracer molecules which remain intravascular throughout their residence in the capillary unit emerge in the transmitted impulse at X = 1, T = 1. This should not be interpreted to mean that tracer molecules in the emerging impulse are confined to the plasma phase. They may cross the erythrocyte permeability barrier any number of times and still be included in the emerging impulse function. However once a tracer molecule crosses the stationary capillary endothelium, it cannot emerge in the transmitted impulse.

The area under the traveling impulse decreases steadily with time since the tracer is always diffusing to an extravascular region at zero concentration. Most of the plasma tracer moves rapidly across the highly permeable capillary endothelium but some of the indicator also diffuses across the erythrocyte membrane into the initially tracer-free red cell phase. However, before the impulse moves 20% of the way through the capillary the mass of indicator in the plasma is depleted to such an extent that the direction of plasma-red cell tracer transport reverses. Thereafter, tracer is transferred from the red cell phase back to the plasma phase where most of it is transported across the capillary endothelium. But the loss of tracer from the red cells is a much slower process than its initial uptake because the concentration gradient is considerably smaller. The final mass of tracer emerging in the red cell phase of the impulse is therefore only slightly less than one half of its maximum value (i.e., near T = .2).

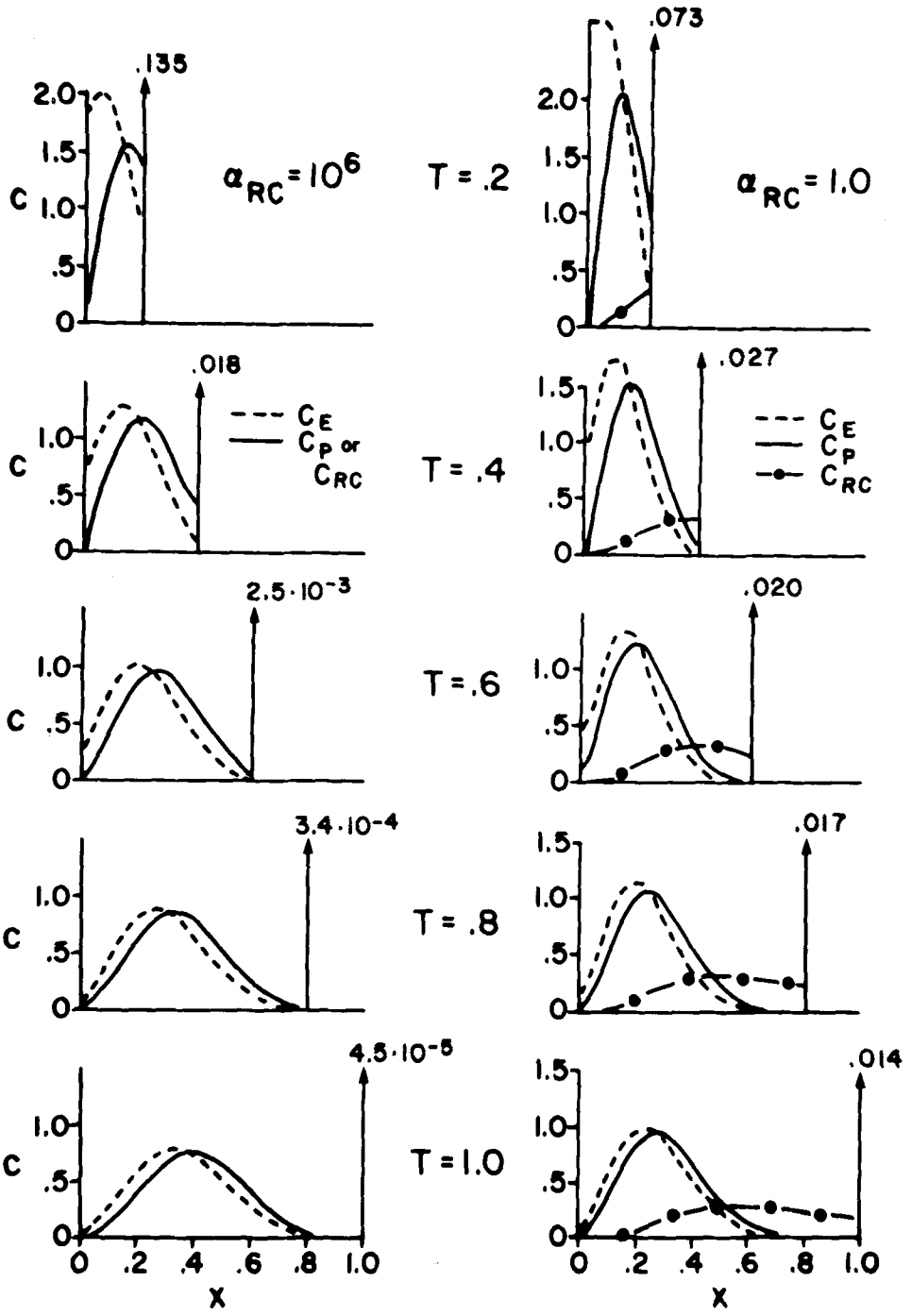

FIGURE 4. Axial tracer distribution at various times after its introduction as an Dirac impulse in the plasma at X = 0 and T = 0; $\alpha_{cap} = 10$, $\beta = .5$, $\gamma = 3$, $\mu = 1$, $\alpha_C \to \infty$. At left: red cells present no barrier to tracer transport ($\alpha_{RC} = 10^6$). Plasma and red cell concentrations are identical at all axial locations. At right: $\alpha_{RC} = 1.0$. Red cell and plasma concentrations are quite different. The number accompanying each impulse spike is the combined plasma and red cell impulse area (initially 1.0) at that time.

An exchange process similar to the one described above for the impulse also occurs in the back-diffusion portion of the $\alpha_{RC} = 1$ curve of Figure 4. Indicator accumulates in red cells as they move through the region of high plasma tracer concentration near the inlet of the capillary. After passing the point where the plasma and red cell concentrations are equal, the red cells begin to lose tracer. Once again this loss will be at a much lower rate than the rate of uptake because the concentration gradient in the exit region of the capillary is relatively small. Due to the trapping of indicator in the red cells, the initial concentration (at X = 1) will be higher and the mean tracer residence time will be shorter (Figure 3). Therefore, for high capillary permeabilities and intermediate red cell permeabilities, neither the impulse area nor the back diffusion portion of the curve will necessarily be confined between the limiting curves $\alpha_{RC} \to 0$ and $\alpha_{RC} \to \infty$.

We may conclude from Figures 3 and 4 that the tracer impulse response can be significantly altered when red cell permeability is finite. The differences are particularly noticeable when capillary permeability is high.

Effects of the Extravascular Cellular Space

Since tracer within the plasma impulse is constantly exposed to an extravascular volume at zero concentration in our ideal capillary unit, the transmitted mass fraction (i.e., emerging impulse area) cannot be altered by changing either the intracellular permeability or either of the extravascular volume ratios γ or ζ. However, the back-diffusion portion of the impulse response will be influenced by any additional permeability barriers present in the extravascular region.

In Figure 5 variations in the impulse response are shown when red cell effects are negligible ($\alpha_{RC} = 1000$) and the dimensionless cellular permeability is varied from 100 to .001. Sixty percent of the extravascular water volume is assumed to be cellular while the remaining portion is occupied by interstitial fluid (i.e., $\zeta = 0.6$). All other parameters are the same as those specified in Figure 3. Less tracer enters the cellular space when cellular permeability is low. Therefore, the smaller the cellular permeability, the higher will be the initial tracer concentration in the back-diffusion portion of the vascular curve. However the same barrier restricts the movement of tracer back into the interstitial space after the concentration gradient reverses. Thus the plasma tracer concentration will eventually fall below the value expected if no cellular barriers existed. This phenomenon is clearly shown in Figure 5 when α_{cap} is 0.15.

The effect of low cellular permeability on the vascular impulse response is even more pronounced when the capillary dimensionless permeability is increased to 10. The peak plasma concentrations occur much earlier when cellular permeability is low than when it is high. In fact when T is less than 3.5, the $\alpha_C = .01$ curve cannot be distinguished from one issuing from a capillary unit having a homogeneous extravascular volume equal to that of

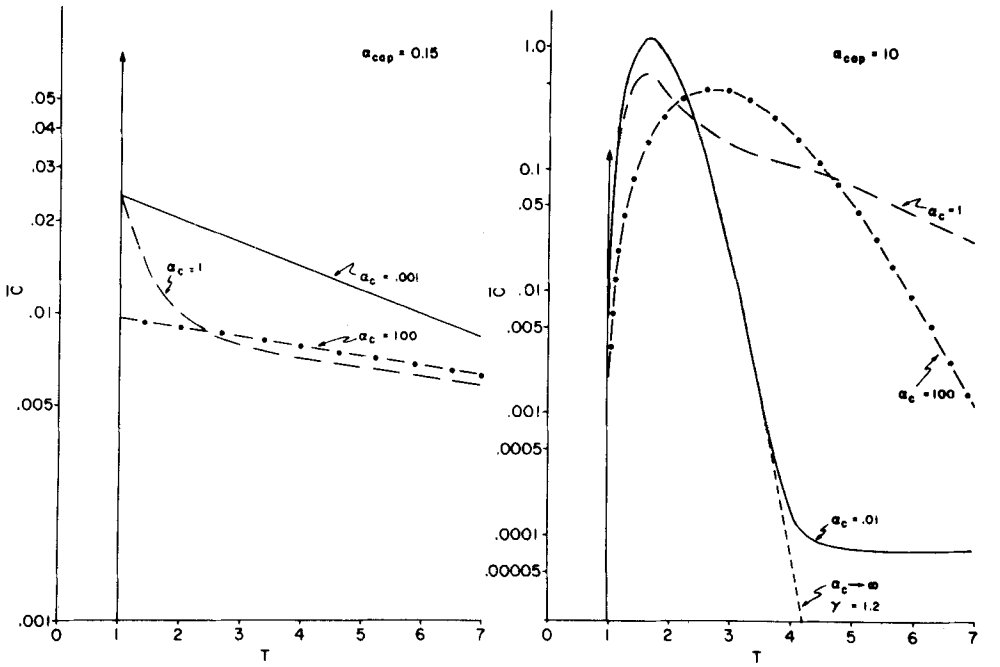

FIGURE 5. Effects of varying dimensionless cellular permeability, α_C, when sixty percent of the extravascular volume is intracellular (i.e. ζ = .6) and $\alpha_{RC} = 10^3$, β = .5, γ = 3, μ = 1, IMAX = 40. Left: α_{cap} = .15. Impulse area for all curves is .861. Right: α_{cap} = 10. Impulse area for all curves is .0002. The homogeneous ($\alpha_C \to \infty$) curve for γ = 1.2 (or alternately α_C = 0, γ = 3, ζ = .6) is shown for comparison with the α_C = .01 curve.

the interstitial fluid volume alone (i.e., where γ is replaced by γ $(1-\zeta)$). Theoretically these two different capillary units could be distinguished by comparing the first moment of their response curves. However the distinction between the two curves is not obvious until $\bar{C}$ falls below .0001 (Figure 5). This would be very difficult to detect experimentally, especially in the presence of recirculation.

Combined Effects

The Sangren-Sheppard model curve (i.e., $\alpha_{RC} \to \infty$, $\alpha_C \to \infty$) is shown in Figure 6 for α_{cap} = 10 and μ = 1. Also drawn for comparison are the curves resulting when the dimensionless red cell permeability alone is finite (α_{RC} = 1) and the dimensionless cellular permeability alone is finite (α_C = 1). The fourth curve in Figure 6 is the impulse response of the same capillary unit when both α_{RC} and α_C are finite ($\alpha_{RC} = \alpha_C = 1$).

The C(T) curve characterizing a capillary unit with finite erythrocyte permeability has a higher initial concentration (excluding impulse) than the corresponding Sangren-Sheppard curve, a lower maximum concentration and the peak is shifted to the right. The initial concentration (i.e., near T = 1) is

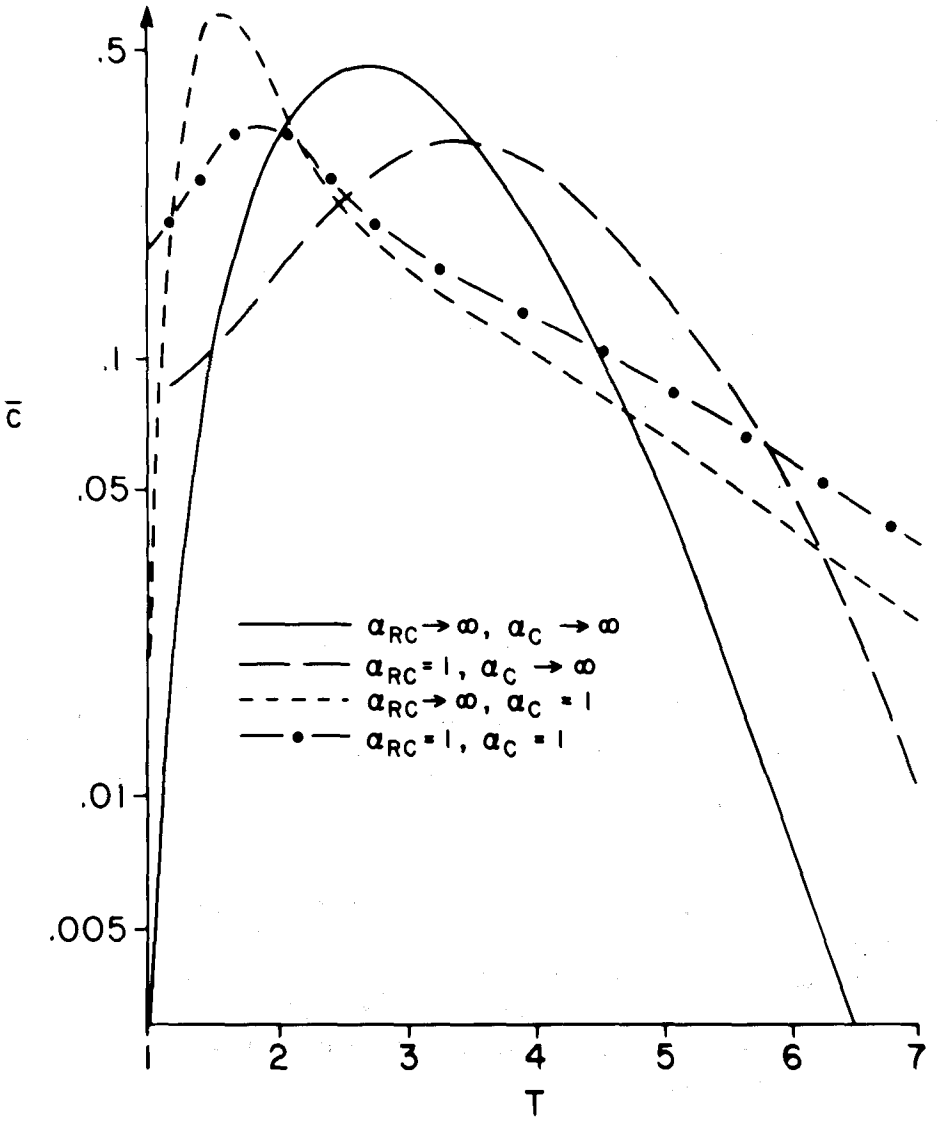

FIGURE 6. Combined effects of red cell and extravascular cellular permeability; $\alpha_{cap} = 10$, $\gamma = 3$, $\zeta = .6$, $\mu = 1$, IMAX = 40. Curves with $\alpha_{RC} \to \infty$ have impulse areas of 4.54×10^{-5}. Curves with $\alpha_{RC} = 1$ have impulse areas of .014.

also higher when cellular permeability is finite, but this increases the maximum concentration, shifts the peak to the left and lowers the final rate at which indicator is removed from the capillary unit.

The C(T) curve which results when both α_{RC} and α_C are unity reflects a combination of the separate effects of each. The initial concentration (excluding impulse) is the highest of the four curves while the terminal washout rate is the slowest of all. Both the location and magnitude of the peak lie

between those for finite α_{RC} alone and finite α_C alone. Generally the non-impulse portion of the curve appears to resemble the curve resulting when α_C alone is finite rather than when α_{RC} alone is finite. The impulse area, on the other hand, is identical to the impulse area resulting when $\alpha_{RC} = 1$ alone and, as was shown earlier, is much higher than the Sangren-Sheppard (or finite α_C) impulse area.

None of the curves with finite α_{RC} or α_C in Figure 6 can be mistaken for the corresponding Sangren-Sheppard curve. However, each might be mistaken for a Sangren-Sheppard curve issuing from a homogeneous capillary unit where γ and α_{cap} differ from the actual values. Thus if either or both of the dimensionless parameters γ and α_{cap} are estimated from a non-homogeneous capillary unit C(T) curve using the homogeneous Sangren-Sheppard model, the estimated parameter values will be in error. The magnitude of the error will depend on each of the dimensionless parameters (α_{cap}, α_C, α_{RC}, β, μ, γ, ζ) and is discussed in detail by Roselli and Harris (12).

NON-IMPULSE INPUT FUNCTIONS

In addition to the impulse response we also determined the tracer response to a more realistic skewed exponential function (Eq. 6b). The resulting dimensionless intravascular reference curve is described by Eq. 15b and is shown in Figure 7 for $\sigma = 1$. Also drawn in Figure 7 for future reference are the Sangren-Sheppard C(T) curves and extraction-time curves for the same input function when $\alpha_{cap} = .15$, 1 and 10.

EXTRACTION

The extraction at the capillary outlet, E, is defined as $E = 1 - \bar{C}(T)/C_R(T)$ and is often used as an indicator of capillary permeability. When back-diffusion can be ignored, Crone (5) has shown that α_{cap} can be determined from the extraction using the following equation:

$$\alpha_{cap} = -\ln(1 - E) = -\ln\left(\frac{\bar{C}(T)}{C_R(T)}\right). \tag{16}$$

In real capillaries extravascular volumes are finite and back-diffusion cannot be ignored. The buildup of tracer in the extravascular region continuously reduces the flux of tracer from the vascular to the extravascular region. Therefore, extraction becomes smaller with time and eventually tracer diffuses back into the vascular region, producing a negative extraction. Generally, then, only the early extraction values (i.e., $T \rightarrow 1$) will produce useful experimental estimates of dimensionless capillary permeability (Figure 7).

We wish now to determine the manner in which the response curves of Figure 7 are altered by: 1) red cell effects, 2) extravascular cellular effects, and 3) dispersion of the input function.

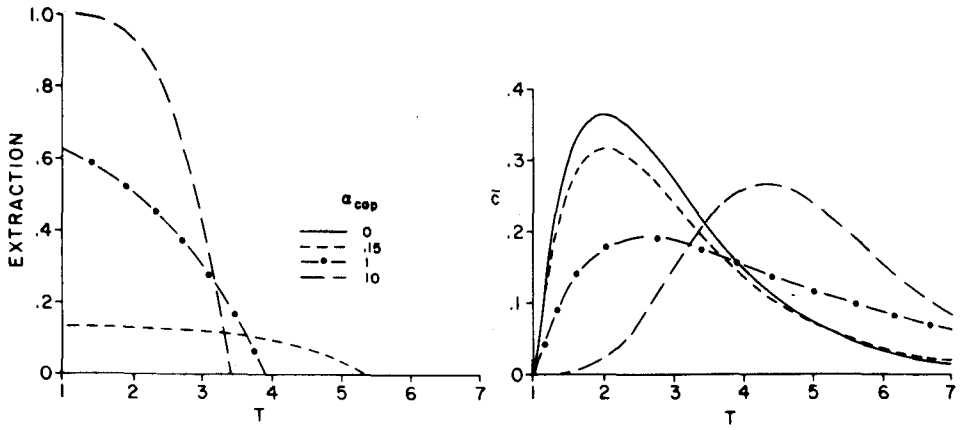

FIGURE 7. Response of Sangren-Sheppard model to our general input function (Eq. 14b) when $\sigma = 1$, $\gamma = 3$. The intravascular reference curve is denoted by $\alpha_{cap} = 0$. Extraction vs. T corresponding to $\alpha_{cap} = .15$, 1.0 and 10 are plotted above the C(T) curves.

EFFECT OF RED CELLS

Red cells can influence transcapillary tracer transport whenever the dimensionless capillary tracer permeability is of the same order of magnitude or larger than the dimensionless red cell permeability. It is clear from the impulse response (Figure 3) that the "red cell effect" is most prominent at low dimensionless red cell tracer permeabilities, high capillary permeabilities and high hematocrit values. In addition, the initial plasma-red cell tracer distribution and the shape of the input curve can significantly alter the extraction patterns.

Red Cell Permeability

In Figure 8 we show the effects of changing the dimensionless red cell tracer permeability, α_{RC}, for a pre-equilibrated injectate. When $\alpha_{cap} = .15$ (not shown) there is very little difference between low red cell permeability ($\alpha_{RC} = .001$) and high red cell permeability ($\alpha_{RC} = 999$) $\bar{C}(T)$ curves. Most of the tracer molecules initially deposited in the erythrocytes cannot permeate the red cell membrane let alone the capillary barrier before emerging from the capillary. The trapping effect is more pronounced when the dimensionless capillary permeability is increased to unity (Figure 8a). The maximum extraction in this case is reduced to about 0.5 when $\alpha_{RC} = .001$ rather than the value of 0.62 found when the red cells are infinitely permeable. The effect of low red cell permeability on the $\bar{C}(T)$ curve and extraction pattern is most pronounced when the capillary permeability is high (Figure 8b). As in the cases where $\alpha_{cap} = .15$ or $\alpha_{cap} = 1$, very little tracer escapes from the red cells when $\alpha_{cap} = 10$ and $\alpha_{RC} = .01$. Both plasma and red cell concentrations are shown for this case in Figure 9. In contrast to the

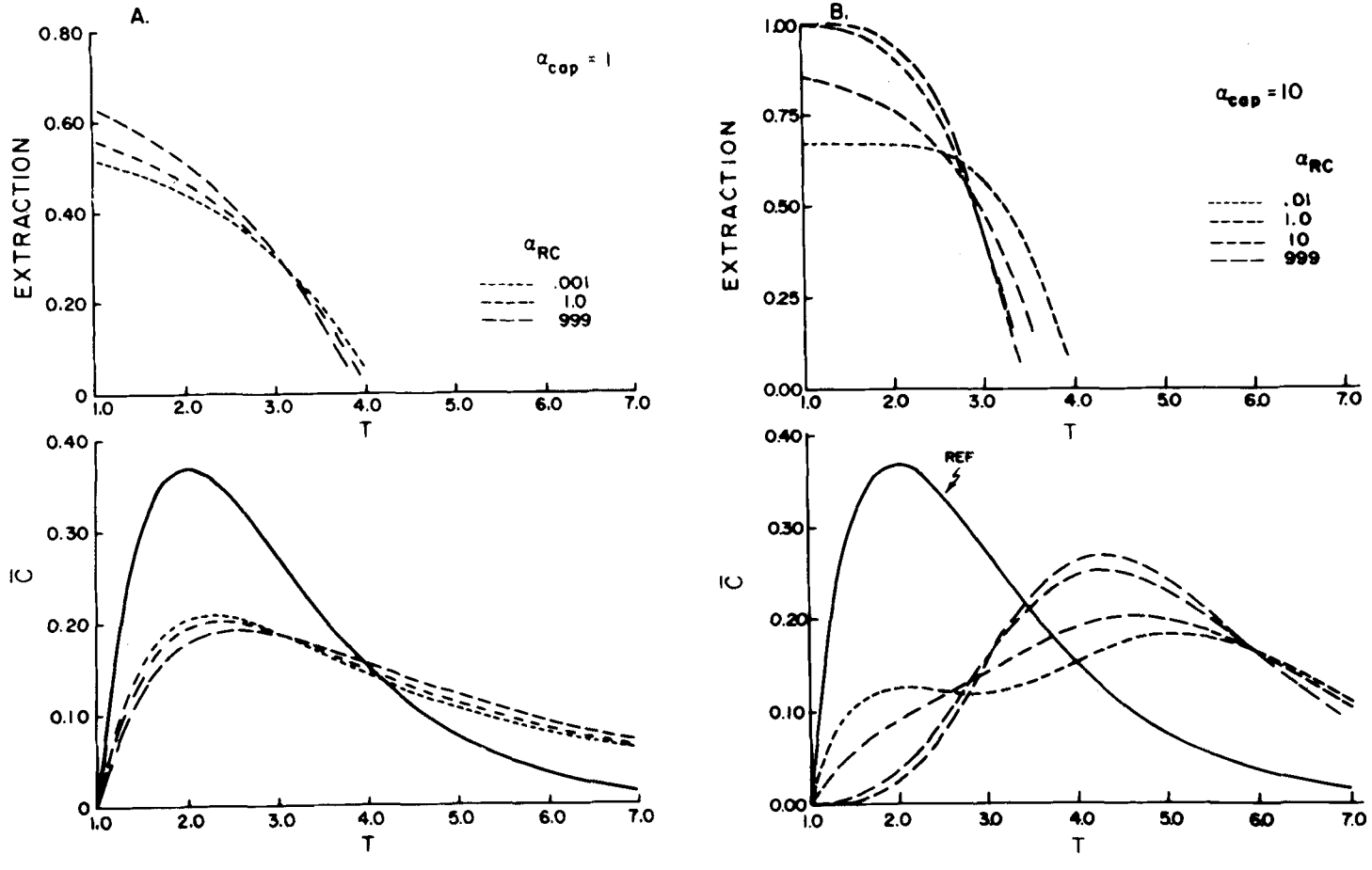

FIGURE 8. Effect of red cell permeability: $\mu = .6667$, $\beta = .5$, $\gamma = 3$, $\alpha_C \to \infty$, IMAX = 80. 8A: $\alpha_{cap} = 1$. 8B: $\alpha_{cap} = 10$. Solid line is the intravascular reference curve ($\sigma = 1$).

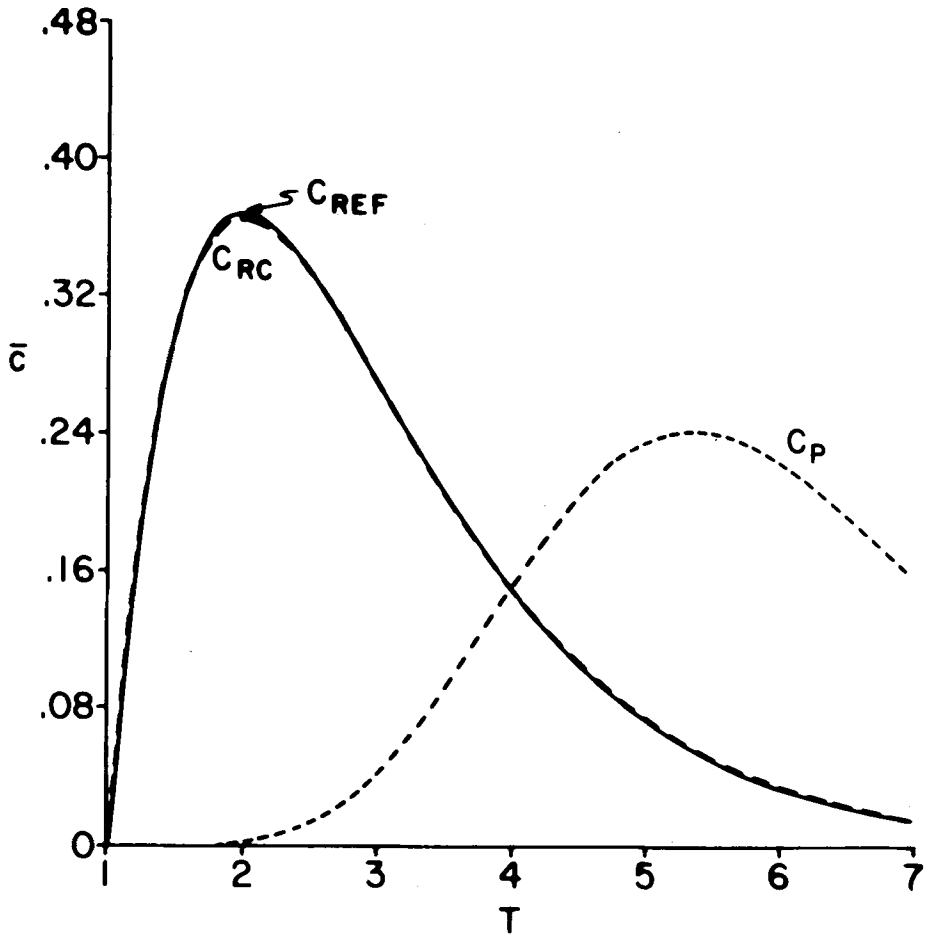

FIGURE 9. Comparison of red cell concentration C_{RC}, plasma concentration C_P, and the intravascular reference curve C_{REF} when $\alpha_{cap} = 10$, $\alpha_{RC} = .01$, $\mu = .6667$, $\beta = .5$, $\gamma = 3$, $\alpha_C \to \infty$, $\sigma = 1$ and IMAX = 80.

previous examples, nearly all of the plasma indicator diffuses into the extravascular space. Therefore the composite vascular curve (Figure 8b) has two peaks which result from combining the red cell curve, which has the same shape as the reference curve, and the plasma curve, which is shifted to the right and more dispersed because of the additional time spent by the tracer molecules in the extravascular volume.

Initial Plasma-Red Cell Tracer Distribution

Low red cell permeability has very little effect on the $\bar{C}(T)$ curve or the extraction pattern when the tracer is initially pre-equilibrated with the in-

jectate blood sample and α_{cap} is small. This is not true when the tracer is initially introduced into either the plasma phase alone or the red cell phase alone (Figure 10). In the latter case ($\mu = 0$) the flow averaged tracer curve is almost identical to the reference curve so the extraction is nearly zero. When tracer is introduced in the plasma alone ($\mu = 1$) the $\bar{C}(T)$ curve lies below the pre-equilibrated ($\mu = .667$) curve since some tracer is driven across the capillary endothelium by the steeper plasma-interstitial concentration gradient.

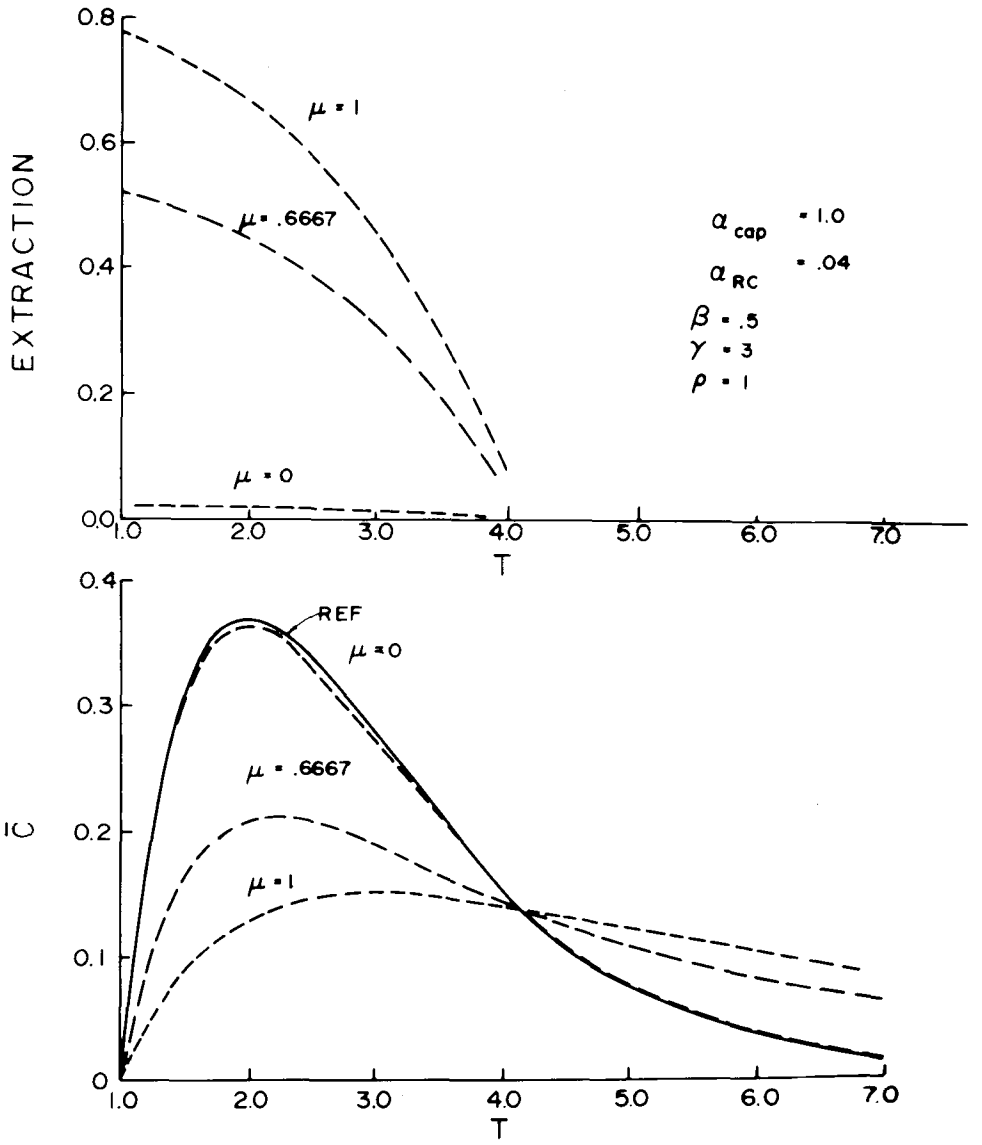

FIGURE 10: Effect on initial plasma-red cell tracer distribution. Tracer is originally in red cells ($\mu = 0$), plasma ($\mu = 1$) or pre-equilibrated ($\mu = .6667$). αcap = 1.0, $\alpha_{RC} = .04$, $\beta = .5$, $\gamma = 3$, $\alpha_c \to \infty$, $\sigma = 1$ and IMAX = 40.

(Note that although the plasma concentration is higher in the $\mu = 1$ case than the pre-equilibrated case, the red cell concentration is nearly zero so that the flow-averaged concentration, $\bar{C}$, is lower than in the pre-equilibrated case). When $\alpha_{RC} = .04$ and $\alpha_{cap} = 1$, the extraction is about 60% higher than in the pre-equilibrated case. When the dimensionless capillary permeability is low ($\alpha_{cap} = .15$) this difference is reduced to slightly more than 30%.

Of particular experimental interest is the comparison between the dimensionless capillary permeability calculated from the early extraction values (using a pre-equilibrated injectate with low red cell permeability; $\alpha_{RC} = .04$) and the actual imposed dimensionless capillary permeability. If α_{cap} is .15 or less, the predicted value is within 4% of the actual value. The percent deviation increases to 27% when α_{cap} is 1.

Hematocrit Value

If red cells interfere with transcapillary tracer transport at one hematocrit value, then the effect will be more pronounced at a higher hematocrit value. We examined the effect of changing the hematocrit value from zero to 60% while keeping the injectate pre-equilibrated and the red cell permeability low. The extraction and $\bar{C}(T)$ curves are only minimally affected by changes in hematocrit value at low dimensionless capillary permeabilities ($\alpha_{cap} < .3$). The effect becomes more important when α_{cap} is increased to unity, where the extraction is considerably reduced when the hematocrit is increased from 0 to 60%. The effects of low red cell permeability become most evident at high hematocrit values and high dimensionless capillary permeabilities where extraction may become almost completely dictated by hematocrit value.

EFFECT OF EXTRAVASCULAR CELLS

Cellular Permeability

In Figure 11 we show the effects of changing the extravascular cellular tracer permeability from .001 to 999 when 60% of the extravascular volume is cellular, $\gamma = 3$ and $\alpha_{cap} = 1$. When cellular permeability is very low the $\bar{C}(T)$ curve is essentially the same as one produced from a homogeneous extravascular volume with $\gamma = 1.2$ (i.e. one where the cellular compartment is completely impermeable). Deviations between these two curves would not be apparent until times much later than $T = 7$ and they probably could not be distinguished experimentally. Thus the extraction patterns for the $\alpha_C = .001$ and $\alpha_C = 999$ curves are as one would expect by accounting for the volume effect alone. The extraction pattern using an intermediate cellular permeability (i.e. $\alpha_C = 1$) behaves initially like the $\alpha_C = .001$ curve but eventually its extraction actually exceeds the extraction of the high cellular permeability case. Such behavior cannot be due simply to a smaller volume of distribution and is attributed to non-uniform exchange in the extravascular region.

Cellular Volume Fraction

The effects of changing the cellular fraction in the extravascular region (i.e., ζ) from 0 to 0.9 when the cells are only slightly permeable were also explored. As in Figure 11, the observed effects seen while $T < 7$, $\alpha_{cap} = 1$ and $\alpha_C = .01$, were almost entirely due to cellular volume exclusion and were

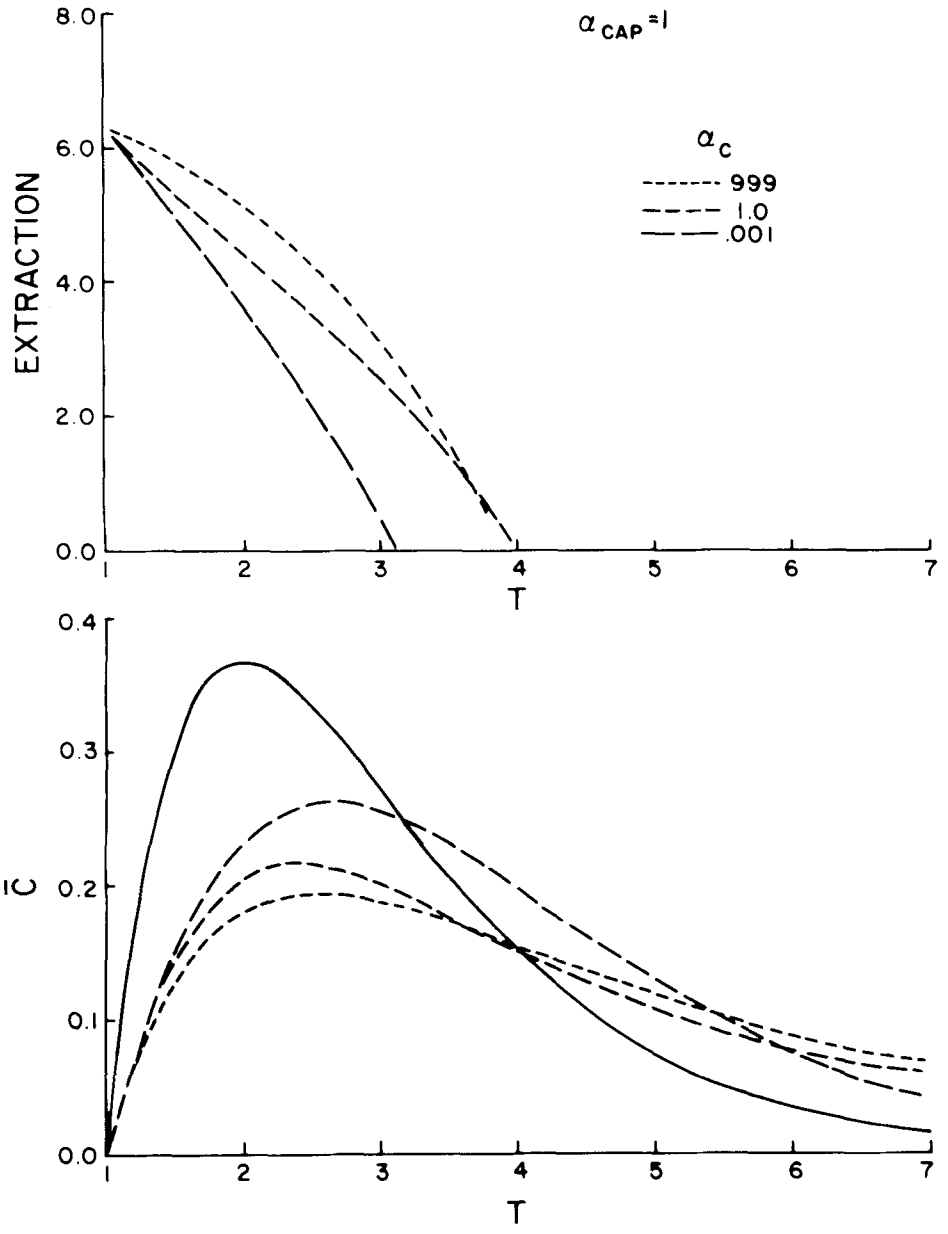

FIGURE 11. Effect of changing cellular permeability when cells comprise 60% of the extravascular water volume ($\zeta = .6$) and $\alpha_{cap} = 1$, $\gamma = 3$, $\alpha_{RC} = 999$, $\sigma = 1$ and IMAX = 40.

not significantly distorted by back diffusion from the slightly permeable cellular region. The variation in the response when the extravascular cellular volume is changed for high dimensionless capillary permeability (i.e., α_{cap} = 10) and a dimensionless cellular permeability of unity is more significant. In that case, each of the non-zero ζ curves crossed the $\zeta = 0$ curve (i.e., homogeneous extravascular regions) before crossing the reference curve, indicating that the response was not simply due to volume-exclusion.

DISPERSION OF THE REFERENCE CURVE

Transcapillary tracer exchange will also be affected by the dispersivity of the input curve, independently of capillary, red cell or intracellular effects. When a major fraction of the tracer enters the capillary in a time interval shorter than the vascular mean transit time, then a high concentration gradient exists across the capillary membrane and a large fraction of the tracer moves into the interstitial space. On the other hand, if the tracer is so dispersed by the time it reaches the capillary level that it takes many capillary transit times for the tracer to enter the capillary, then the relationship between the reference curve and the diffusible curve will be quite different (Figure 12). In this case the plasma-interstitial concentration gradient is initially much smaller and the buildup of tracer in the extravascular region causes the extraction to diminish to a small percentage of its initial value by the time the peak of the reference curve emerges from the capillary.

Comparing the curves in Figure 12 can be misleading because the time scales are different. If the time scales were the same, extraction for the highly dispersed input curve would actually be higher than that of the more pulse-like input curve. However, in practice investigators often use "integral extraction" as a characteristic of capillary permeability. This is obtained by integrating the diffusing and reference curves from the appearance time to the peak time of the reference curve; then inserting the integrated concentrations, rather than the instantaneous concentrations, into Eq. 16. Clearly, from Figure 12 the integral extraction obtained when the reference curve is dispersed would be much smaller than that when the reference curve is more pulse-like. This is true even though the capillary permeability, red cell permeability and cellular permeability are the same in both cases. It is possible then that significant underestimates of capillary permeability may result when the integral extraction method is used to analyze data where the dispersion of the reference curve is large in comparison with vascular capillary transit time. However, it is not likely that this would pose a problem during the collection of multiple-indicator data since the mean transit time of the injected bolus is not two orders of magnitude larger than the intravascular transit time for a single representative capillary.

DISCUSSION

Dimensionless Parameters

Although the maximum number of independent dimensionless parameters associated with the system of Eqs. 1-6 is invariant, our particular choice of dimensionless parameters is not unique. Different dimensionless parameters can always be defined by multiplying or dividing one independent dimensionless parameter by another. For instance under certain circumstances a more convenient parameter than α_C or α_{cap} may be defined by dividing the first by the second. The new parameter, $P_C S_C / P_{cap} S_{cap}$ does not depend on the flow and can be used as an independent parameter in place of either of the dimensionless parameters which were combined to define it.

The red cell permeability-capillary permeability ratio is not simply the ratio α_{RC}/α_{cap}, since the surface areas and flows in the definitions of α_{RC} and α_{cap} are not identical. When the red cells and plasma move through the capillary at the speed this ratio becomes:

$$\frac{P_{RC}}{P_{cap}} = \frac{S_{cap}}{V_{cap}} \frac{V_{RC}}{S_{RC}} \frac{\alpha_{RC}}{\alpha_{cap}} = \frac{1}{f_B} \frac{S_{cap}}{V^*_{cap}} \frac{V_{RC}}{S_{RC}} \frac{\alpha_{RC}}{\alpha_{cap}}$$

V^*_{cap} is the physical volume of the capillary (to be distinguished from

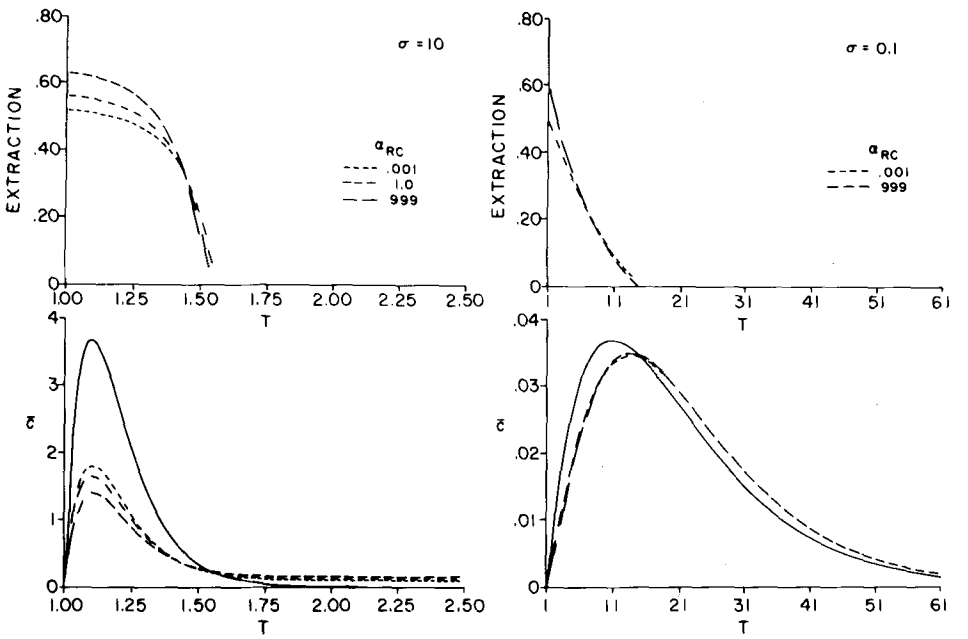

FIGURE 12. Effect of dispersion of the input curve. Left: $\sigma = 0.1$. Right: $\sigma = 10$. For both curves $\alpha_{cap} = 1, \mu = .6667, \beta = .5, \gamma = 3, \alpha_C \to \infty$.

V_{cap} which is the water volume of the capillary) and f_B is the water fraction of the blood:

$$f_B = f_{RC}\,Hct + (1-Hct)\,f_p.$$

The ratio of the membrane surface to the intracellular water volume (S_{cap}/V^*_{cap}) is a constant for red cells. Goresky et al. (6) have calculated this to be 24,324 cm^{-1} for canine erythrocytes. The surface to intracapillary volume ratio is also relatively constant. For a cylindrical capillary, this is simply $2/R_{cap}$ where R_{cap} is the radius of the capillary. If the capillary radius is assumed to be 4 micrometers and the hematocrit is 40%, then:

$$\frac{P_{RC}}{P_{cap}} \simeq .24\,\frac{\alpha_{RC}}{\alpha_{cap}}\,.$$

The figures presented in the previous section with $\alpha_{RC} = .04$ and $\alpha_{cap} = 1$, for example, can alternately be associated with a tracer-capillary system where $\alpha_{cap} = 1$ and $P_{RC}/P_{cap} = .01$.

Pre-Equilibration Time

The model results indicate that if a tracer is erroneously assumed to distribute equally well in both plasma and erythrocytes, the resulting $\bar{C}(T)$ curves will be significantly different from the Sangren-Sheppard curve only when α_{cap} is larger than α_{RC}. On the other hand, for a tracer modeled as though it were totally excluded from red cells, significant deviations from the expected Sangren-Sheppard curve can only arise when α_{RC} is of the same order of magnitude or larger than α_{cap}.

One might argue that a tracer, having a low erythrocyte permeability which is deposited in the plasma phase of a blood sample only minutes prior to injection, would cause only minor errors in multiple indicator capillary permeability estimates. However a short calculation will show that this is not necessarily true. The time constant associated with the resistance of the erythrocyte membrane is:

$$\tau = 1/(1+\beta)\,P_{RC}\,(\frac{S_{RC}}{V_{RC}}).$$

For a relatively impermeable substance such as thiourea ($P_{RC} = .7 \times 10^{-6}$ cm/sec) at room temperature, and a blood sample with a hematocrit value of 40%, the time constant is approximately 40 seconds. After three time constants (i.e., 2 minutes in this example) the plasma and red cell concentrations in the injectate would be very close to their equilibrium values. On the other hand, for a mean capillary transit time of 1 second, a characteristic value of α_{RC} for thiourea would be:

$$\alpha_{RC} = P_{RC}\,(\frac{S_{RC}}{V_{RC}})\,\bar{t} = (.7 \times 10^{-6})\,(24{,}324)\,(1) = .017$$

Therefore it would not be unusual for an indicator, which has been in contact with red cells for only a short time and which has a low α_{RC}, to be nearly pre-equilibrated at the capillary inlet. In fact under experimental conditions tracer molecules, which are injected only in the plasma phase but have time constants of the order of 1 second or less, may have sufficient time during their pre-capillary arterial transit to equilibrate with surrounding red cells before reaching the capillary bed. If capillary permeability is high and capillary transit is less than one second, however, these same cells would interfere with transcapillary transport, leading to an underestimate of capillary permeability using any of the standard multiple indicator techniques.

Extraction

In selected examples we have shown how the flow-averaged concentration-time and extraction-time curves are influenced by variations in characteristic red cell and extravascular parameters. It is not possible to present $\bar{C}(T)$ curves for all or even most combinations of the parameters α_{cap}, γ, μ, α_{RC}, β, α_c, ζ, or σ which may be relevant to experimental determinations of capillary permeability. However the qualitative effects of each parameter and the approximate range over which each influences the extraction can be estimated from the results presented here.

When the dimensionless capillary permeability is low (i.e., $\alpha_{cap} \leqslant .15$) and the injectate is pre-equilibrated, the extraction is only minimally affected if any of the remaining parameters are varied within physiological limits. The only significant deviations from the homogeneous solutions at low α_{cap} occur when the erythrocyte permeability is low and the initial plasma-red cell tracer distribution (μ) is far from the equilibrium value. When a higher percentage of tracer than the equilibrium value is injected in the plasma phase, the extraction will necessarily be higher than in the pre-equilibrated case because the plasma-interstitial concentration gradient is initially steeper. Similarly an initial excess of tracer in the red cells will lead to an extraction-time curve which falls below that of the pre-equilibrated curve.

Generally, the effects of low red cell permeability become more noticeable as capillary permeability is increased. Equilibrating a blood sample with tracer before its introduction at the capillary inlet cannot compensate for the effects of low red cell permeability when capillary permeability is high. The extraction in the vicinity of the appearance time for a pre-equilibrated injectate must be lower when red cell permeability is low than when the tracer easily permeates the erythrocyte membrane (all other conditions remaining unchanged). Therefore, the dimensionless capillary permeability estimated by either the Crone technique or by application of the more sophisticated Sangren-Sheppard model will be lower than the true dimensionless capillary permeability whenever red cells impede trans-endothelial tracer transport. If all the tracer is introduced in the plasma phase and tracer is assumed to be excluded from the red cells, when in fact exchange does

occur across the erythrocyte membrane, then the dimensionless capillary permeability will also be underestimated using standard multiple indicator techniques. Increasing the hematocrit results in even larger underestimates of capillary permeability since a larger fraction of the total tracer mass must be transported in the relatively impermeable red cell phase.

Inhomogeneities in the extravascular region also affect the extraction pattern. However, in the absence of red cell effects, the extraction in the vicinity of the appearance time (i.e., T = 1) depends only on the dimensionless capillary permeability. From T = 1 to the peak of the reference curve, the interstitial concentration rises at a faster rate than the cellular concentration, impeding the extraction of additional tracer molecules. The time interval over which we can obtain accurate estimates of extraction could be significantly shortened if a relatively impermeable intracellular region exists. Obviously, as the ratio of interstitial volume to cellular volume decreases this effect will become even more pronounced and could easily affect capillary permeability estimates, particularly when the integral extraction technique is employed. Use of the integral extraction technique to analyze data where the dispersion of the input function is large in comparison with the capillary vascular transit time, may also lead to a significant underestimate of capillary permeability.

CONCLUSIONS

1. Initial extraction (i.e., extraction as $T \rightarrow 1$) and integral extraction are both influenced by finite red cell permeability. Variations from the Sangren-Sheppard curves are most significant when the dimensionless capillary permeability is high ($\alpha_{cap} \geqslant 1$). Deviations from the Sangren-Sheppard extraction caused by finite erythrocyte permeability, can be kept below 5% when capillary permeability is low (i.e., $\alpha_{cap} \leqslant .15$) by pre-equilibrating the injectate with indicator prior to injection.

2. The initial extraction value (or impulse area in the case of an impulse response) is unaffected by variations in extravascular cellular volume or permeability. However integral extraction will always be lower than the Sangren-Sheppard value because of the additional barrier in the extravascular space. This barrier will cause particularly noticeable $\bar{C}(T)$ variations when α_{cap} is greater than α_C.

3. The initial extraction value is not affected by the dispersion of the input function. However, if the dispersion is very large the integral extraction will be considerably smaller than when the input function is pulse-like.

APPENDIX

Finite Difference Technique

The finite difference scheme used to obtain approximate solutions to the system of partial differential equations (Eqs. 9-14) is briefly presented here.

The method is very similar to that attributed to J. L. Stephenson and used by Bassingthwaighte (1) to examine the effects of axial diffusion and axial variations in capillary permeability on the basic Sangren-Sheppard model. This was chosen over more standard techniques for solving systems of hyperbolic and parabolic partial differential equations (16) because of its greater accuracy in describing the response to a pulse-like input function.

The cellular, interstitial, plasma and red cell regions were each divided along the capillary axis into an equal number of finite element compartments (IMAX). Tracer exchange was artificially split into two consecutive but independent processes: 1) axial tracer movement via convection in the vascular region, followed by 2) membrane limited radial tracer transport between the four concentric compartments (red cell, plasma, interstitial and cellular) at each finite element position. Since axial tracer movement is by convection alone, this can be accomplished by moving the tracer concentration in each red cell and plasma elemental compartment forward to the next axial position in a time interval, Δx, which is equal to the distance traveled, Δx (i.e. L/IMAX) divided by the fluid velocity, u. In demensionless terms the increments are identical:

$$\Delta X = \frac{\Delta x}{L} = \frac{1}{IMAX}$$
$$\Delta T = \frac{\Delta t}{\bar{t}} = \frac{1}{IMAX} \qquad \text{(A1)}$$

The extravascular compartments are stationary. Hence tracer movement by convection from one axial location (j − 1) to the next (j) is described by the following set of equations:

$$C^*_{RC,j}(T+\Delta T) = C_{RC,j-1}(T) \qquad \text{(A2)}$$

$$C^*_{P,j}(T+\Delta T) = C_{P,j-1}(T) \qquad \text{(A3)}$$

$$C^*_{I,j}(T+\Delta T) = C_{I,j}(T) \qquad \text{(A4)}$$

$$C^*_{C,j}(T+\Delta T) = C_{C,j}(T) \qquad \text{(A5)}$$

The asterisks indicate the concentrations in the artificial state assumed to exist after the tracer in the plasma and red cell compartments have been convected to the next axial location but before radial exchange occurs. After moving the contents of each plasma and red cell compartment ahead to the next axial location, we allowed membrane-limited radial tracer transport for a dimensionless time interval ΔT. The following stationary version of Eqs. 9-12 can be written for each set of concentric compartments.

$$\frac{dC_{RC,j}}{dT}(T) = A\left[C_{P,j}(T) - C_{RC,j}(T)\right] \tag{A6}$$

$$\frac{dC_{P,j}}{dT}(T) = B\left[C_{RC,j}(T) - C_{P,j}(T)\right] + C\left[C_{I,j}(T) - C_{P,j}(T)\right] \tag{A7}$$

$$\frac{dC_{I,j}}{dT}(T) = D\left[C_{P,j}(T) - C_{I,j}(T)\right] + E\left[\bar{C}_{C,j}(T) - C_{I,j}(T)\right] \tag{A8}$$

$$\frac{dC_{C,j}}{dT}(T) = F\left[C_{I,j}(T) - C_{C,j}(T)\right] \tag{A9}$$

where

$$A = \alpha_{RC}$$
$$B = \beta\alpha_{RC}$$
$$C = (1+\beta)\,\alpha_{cap}$$
$$D = \frac{(1+\beta)\,\alpha_{cap}}{\gamma(1-\zeta)}$$
$$E = \frac{(1+\beta)\,\alpha_{C}}{\gamma(1-\zeta)}$$
$$F = \frac{(1+\beta)\,\alpha_{C}}{\zeta\gamma}$$

We should point out that the parameters A, B, C, D, E, and F in Eqs. A6-A9 are identical for each compartment and hence the equations are independent of the number of compartments chosen. This is because the surface to volume ratio of each region in each compartment is identical to the surface to volume ratio of the same region for the capillary as a whole. Although the equations are independent of IMAX the solution to the equations (and therefore the accuracy of the finite difference method) does depend on the number of compartments used. The solution to Eqs. A6-A9 with initial conditions (Eqs. A2-A5) at $T = T^* + \Delta T$ can be found using Laplace transforms. The concentrations after radial exchange but before the next convective step are:

$$C_{P,j}(T^*+\Delta T) = a_{11}C^*_{P,j}(T^*) + a_{12}C^*_{RC,j}(T^*) + a_{13}C^*_{I,j}(T^*) + a_{14}C^*_{C,j}(T^*)$$

$$C_{RC,j}(T^*+\Delta T) = a_{21}C^*_{P,j}(T^*) + a_{22}C^*_{RC,j}(T^*) + a_{23}C^*_{I,j}(T^*) + a_{24}C^*_{C,j}(T^*) \tag{A10}$$

$$C_{I,j}(T^*+\Delta T) = a_{31}C^*_{P,j}(T^*) + a_{32}C^*_{RC,j}(T^*) + a_{33}C^*_{I,j}(T^*) + a_{34}C^*_{C,j}(T^*)$$

$$C_{C,j}(T^*+T) = a_{41}C^*_{P,j}(T^*) + a_{42}C^*_{RC,j}(T^*) + a_{43}C^*_{I,j}(T^*) + a_{44}C^*_{C,j}(T^*)$$

where:

$$a_{11} = ADFA_0 + (S_1+A)^*G(S_1)A_1 + (S_2+A)G(S_2) + (S_3+A)G(S_3)A_3$$
$$a_{12} = B[DFA_0 + G(S_1)A_1 + G(S_2)A_2 + G(S_3)A_3]$$
$$a_{13} = C[AFA_0 + (S_1+A)(S_1+F)A_1 + (S_2+A)(S_2+F)A_2 + (S_3+A)(S_3+F)A_3]$$
$$a_{14} = CE[AA_0+(S_1+A)A_1 + (S_2+A)A_2 + (S_3+A)A_3]$$
$$a_{21} = A[DFA_0 +G(S_1)A_1 + G(S_2)A_2 + G(S_3)A_3]$$
$$a_{22} = AB[DFA_0/A + G(S_1)A_1/(S_2+A) + G(S_2)A_2/(S_2+A) + G(S_3)A_3/(S_3+A)]$$
$$a_{23} = AC[FA_0 + (S_1+F)A_1 + (S_2+F)A_2 + (S_3+F)A_3]$$
$$a_{24} = ACE[A_0 + A_1 + A_2 + A_3]$$
$$a_{31} = D[AFA_0 + (S_1+F)(S_1+A)A_1 + (S_2+F)(S_2+A)A_2 + (S_3+F)(S_3+A)A_3]$$
$$a_{32} = BD[FA_0 + (S_1+F)A_1 + (S_2+F)A_2 + (S_3+F)A_3]$$
$$a_{33} = CD\left[\frac{AFA_0}{D} + \frac{(S_1+A)(S_1+F)^2A_1}{G(S_1)} + \frac{(S_2+A)(S_2+F)^2A_2}{G(S_2)} + \frac{(S_3+A)(S_3+F)^2A_3}{G(S_3)}\right]$$
$$a_{34} = CDE\left[\frac{AA_0}{D} + \frac{(S_1+A)(S_1+F)A_1}{G(S_1)} + \frac{(S_2+A)(S_2+F)A_2}{G(S_2)} + \frac{(S_3+A)(S_3+F)A_3}{G(S_3)}\right]$$
$$a_{41} = FD[AA_0 + (S_1+A)A_1 + (S_2+A)A_2 + (S_3+A)A_3]$$
$$a_{42} = BDF[A_0 + A_1 + A_2 + A_3]$$
$$a_{43} = CDF\left[\frac{AA_0}{D} + \frac{(S_1+A)(S_1+F)A_1}{G(S_1)} + \frac{(S_2+A)(S_2+F)A_2}{G(S_2)} + \frac{(S_3+A)(S_3+F)A_3}{G(S_3)}\right]$$
$$a_{44} = CDEF\left[\frac{AA_0}{FD} + \frac{(S_1+A)A_1}{G(S_1)} + \frac{(S_2+A)A_2}{G(S_2)} + \frac{(S_3+A)A_3}{G(S_3)}\right]$$

and:

$$G(S_n) = S_n^2 + (D + E + F)S_n + DF$$

$$A_0 = \frac{-1}{S_1 S_2 S_3}$$

$$A_1 = \frac{e^{S_1\Delta T}}{S_1(S_1-S_2)(S_1-S_3)}$$

$$A_2 = \frac{e^{S_2\Delta T}}{S_2(S_2-S_1)(S_2-S_3)}$$

$$A_3 = \frac{e^{S_3\Delta T}}{S_3(S_3-S_1)(S_3-S_2)}$$

S_1, S_2 and S_3 are the roots of the cubic equation:

$$S^3 + S^2(A+B+C+D+E+F) + S[(A+B)(D+E+F) + C(A+E+F) + DF] + (A+B)DF + (E+F)AC = 0 \quad \text{(A11)}$$

These roots were computed using the International Mathematical and Statistical Libraries (IMSL) Library 1 Subroutine ZRPOLY.

Normally we used 40 to 80 axial compartments for each region. All compartments were initially set at zero concentration. The dimensionless concentrations in the first plasma compartment and first red cell compartment were then set at:

$$C^*_{P,1}(0) = \mu\,(1+\beta)\,\mathrm{IMAX}$$

$$C^*_{P,1}(T\neq 0) = 0$$

$$C^*_{RC,1}(0) = (1-\mu)\frac{(1+\beta)}{\beta}\,\mathrm{IMAX}$$

$$C^*_{RC,1}(T\neq 0) = 0$$

to approximate an impulse input or were set at:

$$C^*_{P,1}(T) = \mu\,(1+\beta)\,\sigma^2 T e^{-\sigma T}$$

$$C^*_{RC,1}(T) = (1-\mu)\frac{(1+\beta)}{\beta}\,\sigma^2 T e^{-\sigma T}$$

for the more general input function. The tracer was then allowed (mathematically) to diffuse radially in all compartments for a dimensionless time interval, 1/IMAX. The corresponding concentrations at the end of this period are found using Eq. A10. Next, the concentration in each red cell and plasma compartment was shifted to the next axial location where radial transport between the four phases was again initiated. This two-step (convection-diffusion) procedure was repeated until the concentration-time histories in the final compartment were sufficiently defined.

TABLE OF NOMENCLATURE

c	tracer concentration (g/ml)
$c_{p,i}$, $c_{RC,i}$	constants. (*See* equations prior to Eq. 7)
c_{po}, c_{RCo}	input concentrations $c_p(t,0)$, $c_{RC}(t,0)$
C	dimensionless tracer concentrations, $\frac{cF\bar{t}}{m_i}$
E	extraction, $1-\bar{C}(T,1)/C_R(T,1)$
f	water fraction
F	water flow (ml/sec)
Hct	hematocrit value
IMAX	number of finite element compartments
L	capillary length (cm)
m	mass of tracer which emerges at T = 1 at capillary outlet
m_i	mass of tracer injected in blood at X = 0
P	permeability (cm/sec)
S	surface area (cm^2)
t	time (sec)

$\bar{t}$	mean capillary transit time, L/u
T	dimensionless time, $t/\bar{t}$
u	plasma and erythrocyte velocity (cm/sec)
V	water volume
V^*_{cap}	physical volume of capillary, V_{cap}/f_B
x	axial position from capillary inlet (cm)
X	dimensionless axial position, x/L

Subscripts

B	blood
cap	capillary
C	cellular
I	interstitial
P	plasma
R	reference
RC	erythrocyte

Superscript

$\bar{}$	flow averaged value

Greek Symbols

α_{cap}	dimensionless capillary permeability, $P_{cap}S_{cap}/F$
α_C	dimensionless cellular permeability, P_CS_C/F
α_{RC}	dimensionless erythrocyte permeability, $P_{RC}S_{RC}/F_{RC}$
β	ratio of red cell to plasma water volumes, V_{RC}/V_P
γ	ratio of extravascular to plasma water volume, $(V_I+V_C)/V_P$
$\delta(t)$	Dirac impulse function
ΔT	Single compartment dimensionless transit time, I/IMAX
ζ	ratio of cellular to total extravascular volume, $V_C/(V_I+V_C)$
μ	dimensionless inlet tracer distribution, $\frac{m_{i,p}}{m_i}$
σ	parameter which controls the dispersion of the input function.
τ	time constant associated with resistance of erythrocyte membrane

REFERENCES

1. Bassingthwaighte, J. B. A concurrent flow model for extraction during transcapillary passage. *Circ. Res.* 35:483–503.
2. Bellman, R., J. A. Jacquez, and R. Kalaba. Some mathematical aspects of chemotherapy: I. One organ models. *Bull. Math. Biophys.* 22:181–198, 1960.
3. Chinard, F. P., C. A. Goresky, T. Enns, M. F. Nolan, and R. W. House, Trapping of urea by red cells in the kidney. *Am. J. Physiol.* 209:253–263, 1965.

4. Conn, H. L., Jr. and J. S. Robertson. Kinetics of potassium transfer in the left ventricle of the intact dog. *Am. J. Physiol.* 181:319-324, 1955.
5. Crone, C. Permeability of capillaries in various organs as determined by use of the indicator diffusion method. *Acta Physiol. Scand.* 58:292-305, 1963.
6. Goresky, C. A., G. G. Bach, and B. E. Nadeau. Red cell carriage of label. Its limiting effect on the exchange of materials in the liver. *Circ. Res.* 36:328-351, 1975.
7. Goresky, C. A., W. H. Ziegler, and G. G. Bach. Capillary exchange modeling. Barrier-limited and flow limited distribution. *Circ. Res.* 27:739-764, 1970.
8. Guller, G., T. Yipintsoi, A. L. Orvis, and J. B. Bassingthwaighte. Myocardial sodium extraction at varied coronary flows in the dog; estimation of capillary permeability by residue and outflow detection. *Circ. Res.* 37:359-378, 1975.
9. Krogh, A. The rate of diffusion of gases through animal tissues, with some remarks on the coefficient of invasions. *J. Physiol.* 52:391-408, 1919.
10. Leonard, E. F. and S. B. Jorgenson. The analysis of convection and diffusion in capillary beds. In: *Ann. Rev. Biophys. Bioeng.*, edited by L. J. Mullins. Palo Alto: Annual Reviews, Inc., 3:293-339, 1974.
11. Rose, C. P., C. A. Goresky, and G. G. Bach. The capillary and sarcolemmal barriers in the heart. An exploration of labeled water permeability. *Circ. Res.* 401:515-533, 1977.
12. Roselli, R. J. and T. R. Harris. The effects of red cell and tissue exchange on the evaluation of capillary permeability from multiple indicator data. *Ann. Biomed. Eng.* 7:239-282, 1979.
13. Sangren, W. C. and C. W. Sheppard. Mathematical derivation of the exchange of a labeled substance between a liquid flowing in a vessel and an external compartment. *Bull. Math. Biophys.* 15:387-394, 1953.
14. Sheehan, R. M. and E. M. Renkin. Capillary interstitial and cell membrane barriers to blood-tissue transport of potassium and rubidium in mammalian skeletal muscle. *Circ. Res.* 30:588-607, 1972.
15. Tancredi, R. G., T. Yipintsoi, and J. B. Bassingthwaighte. Capillary and cell wall permeability to potassium in isolated dog hearts. *Am. J. Physiol.* 229:537-544, 1975.
16. Von Rosenberg, D. V. *Methods for the Numerical Solution of Partial Differential Equations.* New York: American Elsevier, 1969.
17. Ziegler, W. H. and C. A. Goresky. Transcapillary exchange in the working left ventricle of the dog. *Circ. Res.* 29:181-207, 1971.